# Analytical modeling of corroded RC columns considering flexure-shear interaction for seismic performance assessment

# Analytical modeling of corroded RC columns considering flexure-shear interaction for seismic performance assessment

**Ji-Gang Xu[1], De-Cheng Feng[1], Gang Wu[1*], Demitrios M. Cotsovos[2] and Yong Lu[3]**

[1]Key Laboratory of Concrete and Prestressed Concrete Structures of the Ministry of Education, Southeast University, Nanjing 210096, China

[2]Institute of Infrastructure and Environment, School of Energy, Geoscience, Infrastructure & Society, Heriot-Watt University, Edinburgh EH14 4AS, United Kingdom

[3]Institute for Infrastructure and Environment, School of Engineering, The University of Edinburgh, Edinburgh EH9 3JL, United Kingdom

## Abstract

Corrosion of transverse reinforcement can lead to significant shear capacity deterioration resulting in a ductile-designed reinforced concrete (RC) column to potentially fail in a shear manner. Increased risk of shear failure can be more significant for short shear-critical columns when corrosion occurs. Therefore, shear response can be a particularly important issue in seismic performance assessment of corroded RC columns. An efficient analytical model which can capture the shear capacity deterioration due to corrosion and the flexure-shear interaction behaviors of corroded columns is developed in this work. Corrosion effect on flexural behavior is accounted for through the appropriate modification of steel reinforcement, concrete and bond properties. Shear response is simulated by a new macro zero-length shear spring element, and its shear force-shear deformation relationship is modelled with the Ibarra-Medina-Krawinkler deterioration model that can capture strength and stiffness deterioration as well as pinching behavior. A calibration study is carried out based on a collection of experiments of corroded columns failed in shear. Subsequently empirical formulae for the determination of the modeling parameters of the shear spring are proposed. The proposed model is validated by simulating several corroded columns and compering the predictions obtained with the relevant test data. Results show that the proposed model is able to predict reasonably the overall hysteretic behavior. Corrosion effects on the seismic performance of RC columns are investigated with the proposed model. Results demonstrate that the flexure-shear interaction behaviors should be considered for seismic performance assessment of corroded columns.

**Keywords** Reinforced concrete columns, corrosion effects, shear response, flexure-shear interaction, seismic performance, analytical model

## 1 Introduction

Corrosion of reinforcement has been recognized as a main reason of deterioration of reinforced concrete structures. Due to corrosion, the material properties degrade and structural performance diminishes. In the case of reinforcing steel bars, corrosion results in a reduction of their effective sectional area and their mechanical properties, while also leading to deterioration of the bond performance between reinforcing bars and concrete. Meanwhile, corrosion products can lead to the volumetric expansion of the concrete cover and the development of splitting tensile stresses, resulting in a reduction of the strength of the cover concrete. The degradation of the properties of the transverse reinforcement can also reduce their confinement effect, which in turn can have a detrimental effect on the properties of the core concrete. Thus, the overall structural performance can be adversely affected by corrosion, and for this reason corrosion has become an important issue for engineers and researchers.

The effect of corrosion on seismic performance of concrete columns has attracted much research attention. Various

experimental studies have been conducted to investigate the effects of corrosion on RC columns under cyclic loading. Tests by Meda et al. (2014) and Goksu and Ilki (2016) have shown that the flexural strength and ductility of columns decrease with the increasing levels of corrosion being sustained by the longitudinal reinforcement bars. Similar observations have been reported by Ma et al. (2012) and Yang et al. (2016). The energy dissipation capacity has also been observed to decrease with the increasing of corrosion levels of reinforcements (Ma et al. 2012; Yang et al. 2016). It is worth noting that the aforementioned studies have only focused on the corrosion effects on flexural performance of columns. Columns tested in their studies were ductile-designed or only corroded with longitudinal reinforcements (Meda et al. 2014; Goksu and Ilki 2016), thus these columns failed in flexural manners.

Recent studies (Li et al. 2018; Vu and Li 2018a) have shown that the failure mode of ductile-designed columns could shift from flexural to shear if the transverse reinforcement was highly corroded. In fact, transverse reinforcement can corrode more severely in reality as the diameter is smaller and the distance to corrosive environment is closer compared with longitudinal reinforcement (Vu and Li 2018a). Thus, the shear capacity could deteriorate more significantly as compared with flexural capacity. As a result, columns could fail in shear under cyclic loadings although they were originally designed to fail in flexure. For example, tests by Vu and Li (2018a) showed that a 25% corrosion level in transverse reinforcement could cause a shift of the column failure mode from flexure to shear under a relative low axial load level, and the corrosion level that could cause a failure mode change was be even lower when the column specimen was subjected to high axial load level. Li et al. (2018) also reported that with the corrosion level of transverse reinforcement increasing, failure model could shift from bending to shear. In such cases, once peak shear capacity was attained, significant strength and stiffness degradation were observed, with more serious pinching effect (Vu and Li 2018a). As shear failure is generally more unpredictable and catastrophic, more attention should be paid to shear performance deterioration of corroded columns.

Apart from corrosion in standard ductile-designed RC columns which could result in a change of failure mode, corrosion has also been observed in short shear-critical columns (Ma et al. 2018; Vu and Li 2018b). In these columns the effect of corrosion in promoting shear failure is more critical. Tests conducted by Vu and Li (2018b) showed that corrosion could cause significant shear strength and deformation capacity deterioration of short columns.

Beyond the experimental studies associated with corroded columns, there have also been some numerical researches aiming at investigating the effects of corrosion on the seismic performance of RC structures. Di Carlo et al. (2017a, b) developed a three-dimensional finite-element (FE) model to investigate the behavior of corroded columns under cyclic loadings. Vu et al. (2016) investigated strength and drift capacity of corroded columns based on three-dimensional FE models. Some other numerical studies used fiber beam-column models. Kashani (2014) developed a nonlinear fiber beam-column model that considers corrosion damage effects on the stress-strain relationship of reinforcements. Afsar Dizaj et al. (2017) investigated corrosion effects on seismic damage limit states and residual capacity of concrete columns based on a developed fiber beam-column model. It should be noted that in most of the numerical studies using solid finite-element or fiber beam-column models, the corrosion effects have been simulated through modifications on the material properties and bond behavior, especially concerning the flexural behavior. Little has been done on the modeling of the shear performance deterioration due to corrosion and the subsequent influence on the flexure-shear interaction behaviors under seismic loadings.

In order to account for shear response, the Timoshenko flexure-shear element and macro spring based flexure-shear element are two commonly used methods in numerical modeling. However, the first method relies heavily on the material constitutive model to reflect the element behavior in shear, and it is more computational costly for the analysis of complex structures (Feng et al. 2017; Feng and Xu 2018; Feng et al. 2019a). The second method, on the other hand, is more easy to

apply and computationally more efficient, but requires an appropriate definition of shear force-shear deformation relationship which can be demanding. The models developed by D'Ambrisi and Filippou (1999), Lee and Elnashai (2001), Elwood (2004), Setzler and Sezen (2008), LeBorgne and Ghannoum (2014b), Cassese et al. (2018) fall into the category of the second method. However, so far none of these models has considered shear capacity deterioration in corroded columns.

In summary, it can be stated that the deterioration of the shear resistance is an important issue in seismic performance assessment of corroded columns. A ductile-designed RC column could fail in shear due to corrosion of transverse reinforcement, and the problem with shear can be even more critical in short shear-critical columns in a corroded condition. To enable a reliable analysis of the behavior of corroded RC columns, a computationally-efficient model capable of considering the shear performance deterioration and shear response under seismic loadings is needed. In this paper, an analytical model considering the flexure-shear interaction in corroded RC columns is developed. The model is based on the macro-element concept, and a new zero-length shear spring is introduced in series with a fiber flexural element and a rotational slip element. Thus, the flexural and shear response are coupled at the element level. The hysteretic model for the shear component takes into account the basic cyclic strength and in-cycle strength degradation, stiffness degradation and pinching. Empirical formulae for the modeling parameters of the shear model are developed based on calibration on a corroded column database which is collected from literature and includes corroded RC columns failed in shear. The proposed model is verified with test results of corroded RC columns. Subsequently, the corrosion effects on the seismic performance of RC columns are discussed based on the proposed model.

## 2 Methodology of modeling corroded RC columns including flexure-shear interaction

### 2.1 General

In this study, a two dimensional (2D) nonlinear FE model is developed in OpenSEES (Mazzoni et al. 2006) for simulating seismic behavior of corroded reinforced concrete columns. The model is aimed to simulate not only the flexural behavior but also the shear response.

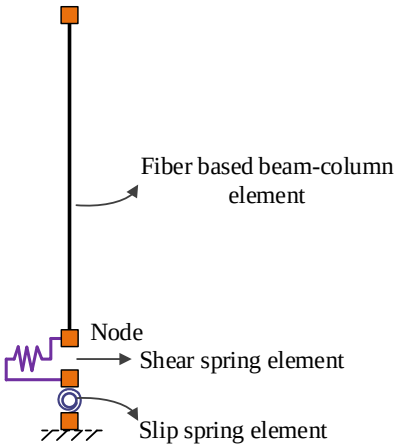


**Fig. 1** Modeling concept of corroded columns in OpenSEES

Fig. 1 shows the modeling concept for a corroded RC column. A fiber-based nonlinear beam-column element is used for simulating the flexural behavior of the column. A zero-length element is added at the end of the column for simulating the bond-slip behavior. Besides, a zero-length element is also added at the end of the column to account for the shear

response. Thus, the multi-mechanism response of a corroded column including flexural behavior, bond-slip behavior and shear behavior is represented at the element level in a coupled manner. The *P-Delta* effects are also explicitly considered.

### 2.2 Flexural behavior

The flexural behavior of the column is modelled with beam-column element assigned with a fiber section. The fiber section is divided into concrete fibers and steel fibers with unique constitutive stress-strain relationship. The material *Steel02* and *Concrete01* in OpenSEES are adopted for simulating the steel reinforcement and concrete, respectively. However, with corrosion, the mechanical properties of materials will change. Thus, in order to accurately simulate the corrosion effects on flexural behavior of columns, the constitutive stress-strain relationship of steel fibers and concrete fibers need to be modified (Fig. 2).

Previous studies (Du et al. 2005a, b) have found that corrosion will reduce the cross-section area and cause yield strength and elastic modulus deterioration of the steel reinforcement. The reduced cross-sectional area can be written as:

$$A_{s,cor} = A_{s0} \cdot (1 - X_{cor}) \tag{1}$$

where $A_{s,cor}$ and $A_{s0}$ are the cross-sectional area of the corroded and uncorroded reinforcement, respectively; $X_{cor}$ is the corrosion level estimated in terms of mass loss.

The strength and elastic modulus degradations are complicated, but in general they are correlated to the degree of corrosion. Thus, the present study adopts the following expressions:

$$f_{y,cor} = f_{y0} \cdot (1 - \alpha_1 \cdot X_{cor}) \tag{2}$$

$$E_{s,cor} = E_{s0} \cdot (1 - \alpha_2 \cdot X_{cor}) \tag{3}$$

$f_{y,cor}$ and $f_{y0}$ are the yield strength of the corroded and uncorroded reinforcement, respectively; $E_{s,cor}$ and $E_{s0}$ are the elastic modulus of the corroded and uncorroded reinforcement, respectively; $\alpha_1$ and $\alpha_2$ are empirical coefficients and are taken to be 0.5 (Du et al. 2005b) and 0.75 (Lee et al. 1998), respectively.

For the cover unconfined concrete, volumetric expansion caused by steel rust will develop splitting stresses in concrete, resulting in reduced concrete strength. In order to consider this adverse effect, a softening coefficient, $\zeta$ , is introduced for the degraded cover concrete strength:

$$f_{c,cor}^{'} = \zeta f_{c}^{'} \tag{4}$$

where $f_{c}^{'}$ and $f_{c,cor}^{'}$ are the compressive strength of cover concrete of the column before and after corrosion, respectively.

According to Hsu and Mo (2010), the softening coefficient can be evaluated by:

$$\zeta = \frac{0.9}{\sqrt{1 + 600\varepsilon_{cr}}} \tag{5}$$

$$\varepsilon_{cr} = \frac{w_{cr}}{b_0} \tag{6}$$

where $\varepsilon_{cr}$ is the tensile strain induced by corrosion cracks; $b_0$ is the circumference of column section; $w_{cr}$ is the total crack width of the column, and this value may be measured in practical engineering or laboratory test. Experimental test results

(Vu and Li 2018b) have suggested that the corrosion induced total crack width actually is well correlated with the transverse reinforcement corrosion level. Thus, the $w_{cr}$ can be estimated indirectly through the corrosion level:

$$X_t = 21.91 w_{cr}(\text{mm}) + 5.34 \tag{7}$$

where $X_t$ is the transverse reinforcement corrosion level.

For the confined core concrete, because of the corrosion of transverse reinforcement, the confinement effect will also decrease. In this study, the modified Kent-Park model (Park et al. 1982) is adopted for calculating the concrete strength of core concrete using deteriorated steel material parameters:

$$K = 1 + \frac{\rho_{st,v} f_{yt,cor}}{f_c^{'}} \tag{8}$$

$$f_{cc,cor}^{'} = K f_c^{'} \tag{9}$$

$$\varepsilon_{cc,cor} = K \varepsilon_c \tag{10}$$

where $K$ is the confinement ratio; $\rho_{st,v}$ is the volume corroded transverse reinforcement ratio; $f_{yt,cor}$ is the yield strength of corroded transverse reinforcement; $\varepsilon_{cc,cor}$ is the peak strain corresponding to the confined core concrete strength $f_{cc,cor}^{'}$.

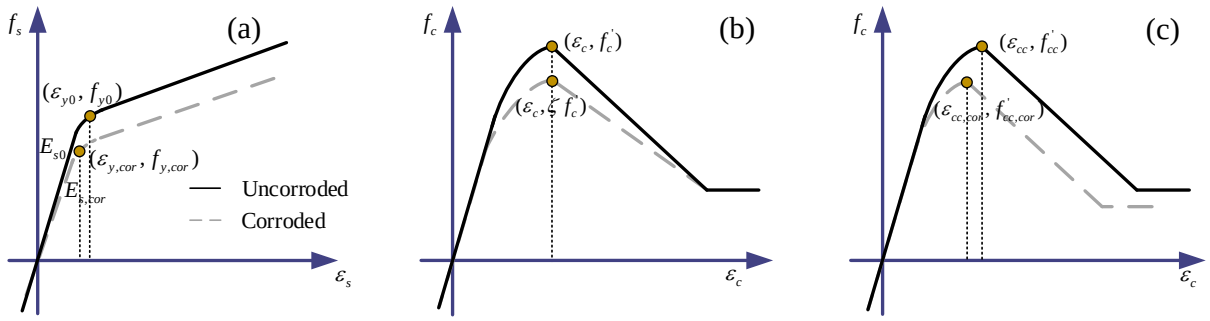


**Fig. 2** Material properties of corroded concrete column: **a** reinforcement; **b** cover concrete; **c** core concrete

### 2.3 Rotational slip behavior

In order to account for the rotational displacement caused by strain penetration or bond slip of the longitudinal steel reinforcements (Feng et al. 2019b), a zero-length rotational slip spring is added at the end of the beam-column element. The elastic stiffness $K_{se}$ of the rotational spring is calculated using the method suggested by Elwood and Eberhard (2009):

$$K_{se} = \frac{8\mu_c}{d_c f_{yl,cor}} \frac{M_y}{\phi_y} \tag{11}$$

where $d_c$ is the diameter of the corroded longitudinal reinforcement; $f_{yl,cor}$ is the yield strength of the corroded longitudinal reinforcement; $M_y$ and $\phi_y$ are the effective yield moment and effective yield curvature of the column section, respectively; $\mu_c$ is the uniform bond stress along the embedded length of the corroded longitudinal reinforcement. Based on Lee et al. (2002), the ratio of bond strength of corroded to uncorroded reinforcement is:

$$\mu_c / \mu = e^{-5.61 X_l} \tag{12}$$

where $X_l$ is the corrosion level of longitudinal reinforcement; $\mu$ is the bond strength for uncorroded reinforcement, and based on Elwood and Eberhard (2009), the $\mu$ can be estimated as below:

$$\mu = 0.8\sqrt{f_c'} \tag{13}$$

The yield moment and yield curvature can be obtained from a cross-sectional analysis in OpenSEES.

### 2.4 Shear behavior

A zero-length shear spring element is added at the end of the column in series with the rotational slip spring element. The shear spring element is used to model the shear behavior of the corroded column. As discussed previously, columns that suffered corrosion may experience shear failure under seismic loadings, leading to significant deterioration in behavior in terms of strength, unloading and reloading stiffness, as well as pinching. The incorporation of the shear spring element makes it possible to represent the complex degradation of the behaviors of corroded columns.

In this study, the modified Ibarra-Medina-Krawinkler deterioration model (IMK) is chosen to simulate the shear behavior of corroded column. This model was developed by Ibarra et al. (2005) and subsequently modified by Lignos and Krawinkler (2008) to address asymmetric hysteretic response. This model has been used by many researchers to model flexural behavior of structural components, including ductile and non-ductile components (Haselton et al. 2011; Liel et al. 2011; Gokkaya et al. 2017). As the model has the ability to represent complex hysteretic deterioration behaviors, it is suitable to model shear behavior of corroded columns. This model has been implemented in OpenSEES by Lignos and Krawinkler (2008).

Fig. 3 shows the primary curve and basic hysteretic rule of the modified Ibarra-Medina-Krawinkler deterioration model with pinched hysteretic behavior. The strength is bounded by the primary curve, including three strength parameters: yield strength $V_y$, peak strength $V_n$ and residual strength $V_r$; and four deformation parameters: yield deformation $\Delta_y$, pre-peak plastic deformation $\Delta_p$, post-peak plastic deformation $\Delta_{pc}$ and ultimate deformation capacity $\Delta_u$. The hysteretic deterioration behaviors is defined by a set of hysteretic rules. In the IMK model, the hysteretic energy based cyclic deterioration rules developed by Rahnama and Krawinkler (1993) are used to define cyclic deterioration rates. The basic strength and post-peak strength deterioration can be calculated as:

$$F_i = (1-\beta_i)\cdot F_{i-1} \tag{14}$$

where $F_i$ and $F_{i-1}$ are strength after and before excursion $i$; $\beta_i$ is an energy-based deterioration parameter calculated as follows:

$$\beta_i = \left(\frac{E_i}{E_t - \sum_{j=1}^{i-1} E_j}\right)^c \tag{15}$$

where $E_i$ is the dissipated energy of excursion $i$; $\sum E_j$ is the total dissipated energy before excursion $i$; $c$ is an empirical parameter and can be taken as 1.0; $E_t$ is the reference hysteretic energy dissipation capacity of specific structural component:

$$E_t = \gamma F_y \Delta_y \tag{16}$$

The parameter $\gamma$ defines the hysteretic energy dissipation capacity of structural components and can be calibrated from experimental results. The same concept is also used to model stiffness deterioration, including accelerated reloading stiffness deterioration and unloading stiffness deterioration. More details of the model can be referred to (Ibarra et al. 2005) and (Lignos and Krawinkler 2011).

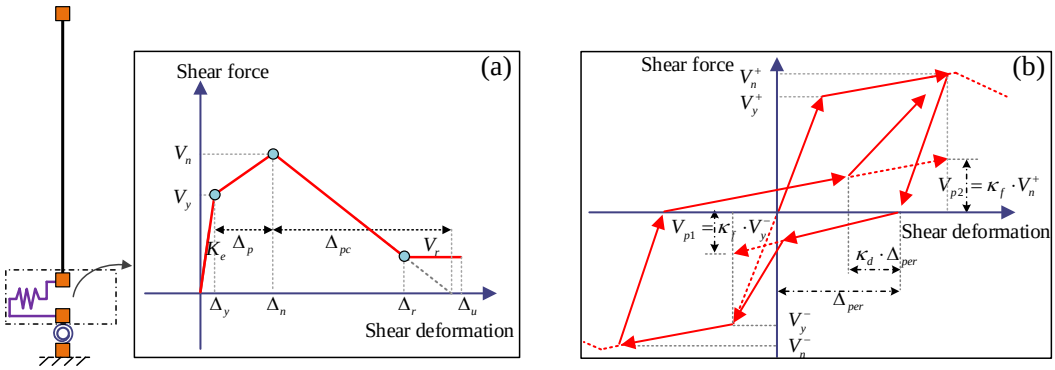


**Fig. 3** Modified IMK model for shear behavior simulation: **a** primary curve; **b** basic hysteretic model rules (adapted from Ibarra et (2005))

### 2.5 Response mechanism of the proposed modeling concept

The proposed model captures shear behavior of corroded column with a macro zero-length element. The flexural behavior, rotational slip behavior, and shear behavior are coupled at element level through equilibrium and compatibility conditions. Under lateral loadings, the shear force of each element will be the same, but the deformation development of each element will be different for different cases.

If the shear capacity $V_n$ of the column is lower than its flexural strength $V_f$, the column will fail in shear. Fig. 4 shows schematically the response development of the column in this failure mode. Before reaching the shear capacity $V_n$, shear response and flexural response develop in accordance with the solid line in the figure at the same time. After the shear demand exceeds shear capacity $V_n$, shear failure occurs and the shear response enters into descending range where singnificant deterioration behavior occurs, consequently the total response is controlled by the shear behavior. The strength of the columns will be bounded by the shear force of the shear element.

If the shear capacity $V_n$ of the clolumn is larger than flexural strength $V_f$, the column will fail in flexure. The response development of the column in this failure mode is shown in Fig. 5. Before the flexural capacity $V_f$, shear response and flexural response develop in accordance with the solid line in the figure at the same time; after the shear demand exceeds flexural capacity $V_f$, flexural failure occurs and the flexural response enters into descending range, and the total response will be controlled by the flexural behavior.

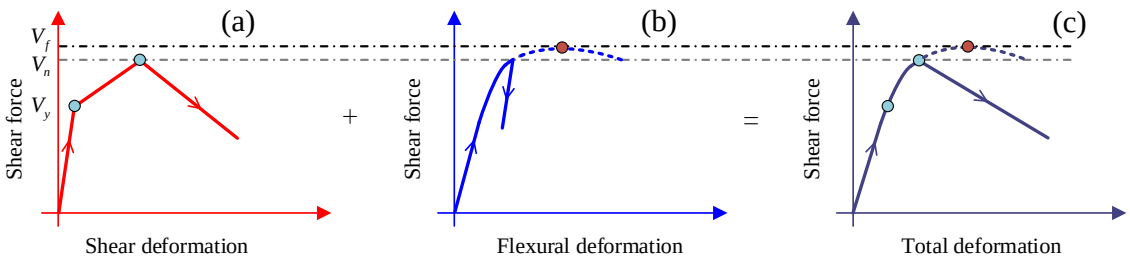


**Fig. 4** Development of each response component in shear failure mode: **a** shear response; **b** flexural response; **c** total response

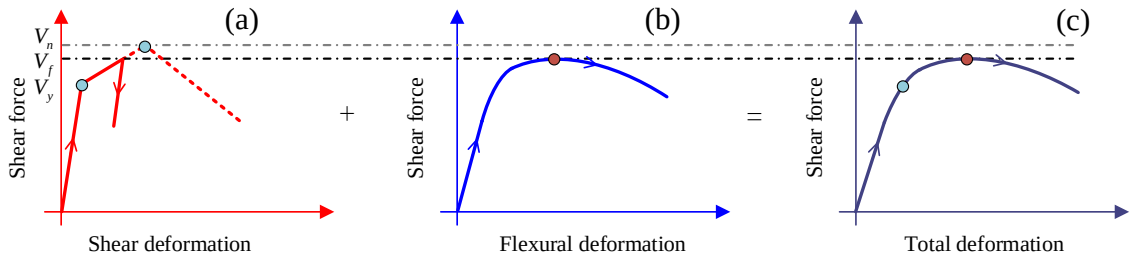


**Fig. 5** Development of each response component in flexural failure mode: **a** shear response; **b** flexural response; **c** total response

## 3 Development of IMK-shear hysteretic model

In order to accurately simulate the shear behavior of corroded columns under seismic loadings with the IMK model, appropriate relationships between the modeling parameters of the IMK model and the corroded column parameters, including geometric or material properties, need to be established. In this section, empirical formulas for the modeling parameters of the IMK model for corroded RC columns will be proposed by calibration against a corroded column database.

### 3.1 Corroded column database

Test data relating to corroded concrete columns is limited, especially for the case of columns failing in shear. Following an extensive literature survey, a total of 25 corroded columns which exhibited shear failure under cyclic loading, have been identified. These columns are summarized in Table 1. The database contains columns which were originally designed to be ductile but failed in shear due to the corrosion of stirrups, and it also contains some short shear-critical corroded columns. In all columns considered, the transverse reinforcement was characterized by a certain level of corrosion. Whereas, on a portion of the specimens considered included longitudinal reinforcement that had also sustained a certain level of corrosion.

The variation ranges of the main parameters of the collected corroded columns are as follows: a) corrosion level (mass loss): longitudinal reinforcement: $0 \le X_l(\%) \le 18$; transverse reinforcement: $4.2 \le X_t(\%) \le 27.2$; b) shear span to depth ratio: $1.9 \le a/d \le 5.3$; c) transverse reinforcement spacing to column depth ratio: $0.178 \le s/d \le 0.784$; d) concrete compressive strength (MPa): $21.0 \le f_c^{'} \le 40.0$; e) reinforcement yield strength (MPa): longitudinal: $395 \le f_{yl} \le 550$; transverse: $235 \le f_{yt} \le 476$; f) reinforcement ratio: longitudinal: $0.0138 \le \rho_l \le 0.0628$; transverse: $0.0017 \le \rho_t \le 0.0093$; and g) axial load ratio ($\nu = P/A_g f_c^{'}$): $0.1 \le \nu \le 0.38$.

### 3.2 Extraction of shear response from column test data

The test data of corroded columns under cyclic loadings have usually been expressed in terms of global shear force-lateral displacement relationship. As the proposed shear spring element is intended to represent the pure shear behavior of a corroded column, the shear response needs to be separated from the global response of the tests in order to fit the shear spring element modeling parameters. To this end, firstly, the flexural analytical model for each column was established with the proposed modeling concept in Section 2, without however the shear spring element. Then, the force history of the column as experienced during the test was imposed to the model to obtain flexural response, including flexural deformation and slip deformation. The shear response was then obtained by subtracting the resulting flexural response (deformation) from the total global response (deformation).

### 3.3 Calibration of IMK modeling parameters for shear response

After obtaining the shear response of each column, calibration of modeling parameters is conducted in order to relate the extracted shear response to the IMK hysteretic model. The strength and deformation parameters of the primary curve described in Section 2.4 can be derived directly from the extracted shear response, while the deterioration and pinching parameters need to be calibrated with trial search in order to best fit the extracted shear response from the experiment. The detailed calibration process for each parameter is described subsequently.

Fig. 6 shows an example of the procedure for column CC1 tested by Vu and Li (2018b), where Fig. 6(a) is the test total response and the extracted flexural and shear response; Fig. 6(b) is the extracted shear response and simulated shear response using calibrated IMK modeling parameters for this column (detailed explanation of the IMK parameter can be referred to subsequent sections); Fig. 6(c) is the simulated global response using the calibrated IMK modeling parameters and it can be seen from these figures that with appropriately calibrated modeling parameters, the shear response can be well reproduced using the IMK hysteretic model, the global response for corroded RC column failed in shear can also be well modeled with the proposed modeling concept.

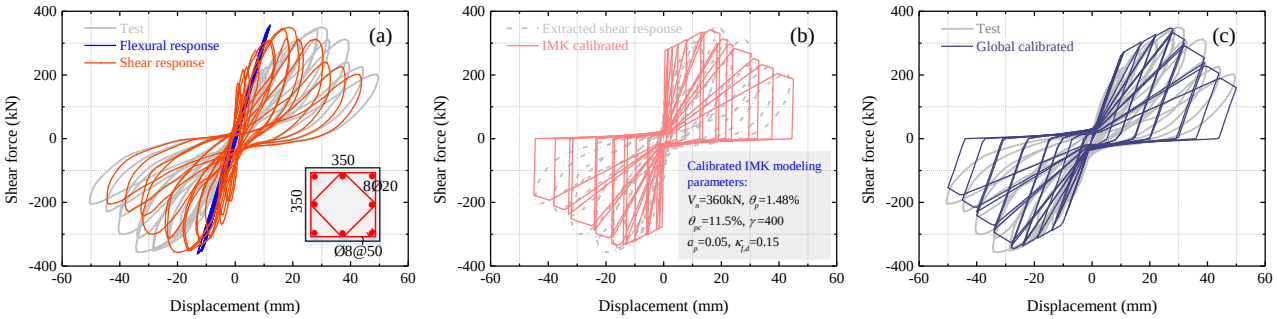


**Fig. 6** Procedure of calibrating IMK modeling prameters: **a** response components extraction; **b** shear response calibration; **c** calibrated global response

**Table 1** Collected corroded column database

| Reference | Specimen | $X_t$ | $X_l$ | $b$ (mm) | $h$ (mm) | $a$ (mm) | $d$ (mm) | $s$ (mm) | $\rho_l$ | $\rho_t$ | $f_c^{'}$ (MPa) | $f_{yl}$ (MPa) | $f_{yt}$ (MPa) | $P$ (kN) | Test type** |
|---|---|---|---|---|---|---|---|---|---|---|---|---|---|---|---|
| Vu and Li (2018b) | CC1 | 11.4 | 3.4 | 350 | 350 | 540 | 280 | 50 | 0.021 | 0.0093 | 28.8 | 550 | 300 | 353 | DC |
| | CC2 | 21.3 | 5.8 | 350 | 350 | 540 | 280 | 50 | 0.021 | 0.0093 | 32.0 | 550 | 300 | 392 | DC |
| | CC3 | 26.1 | 6.8 | 350 | 350 | 540 | 280 | 50 | 0.021 | 0.0093 | 27.8 | 550 | 300 | 341 | DC |
| | CC4 | 8.4 | 3.4 | 350 | 350 | 540 | 280 | 50 | 0.021 | 0.0093 | 34.4 | 550 | 300 | 1054 | DC |
| | CC5 | 12.1 | 3.3 | 350 | 350 | 540 | 280 | 50 | 0.021 | 0.0093 | 31.3 | 550 | 300 | 959 | DC |
| Vu and Li (2018a) | C3 | 25.0 | 10.9 | 350 | 350 | 890 | 280 | 50 | 0.021 | 0.0093 | 40.0 | 550 | 300 | 490 | DC |
| | C4 | 13.6 | 3.4 | 350 | 350 | 890 | 280 | 50 | 0.021 | 0.0093 | 30.0 | 550 | 300 | 918 | DC |
| | C5 | 15.5 | 3.9 | 350 | 350 | 890 | 280 | 50 | 0.021 | 0.0093 | 31.3 | 550 | 300 | 958 | DC |
| Ma et al. (2018) | RN1 | 4.2 | 2.8 | 300 | 300 | 600 | 255 | 200 | 0.014 | 0.0017 | 28.1 | 420 | 310 | 480 | DC |
| | RN2 | 4.9 | 3.2 | 300 | 300 | 600 | 255 | 200 | 0.014 | 0.0017 | 28.1 | 420 | 310 | 600 | DC |
| | RN3 | 4.7 | 3.0 | 300 | 300 | 600 | 255 | 200 | 0.014 | 0.0017 | 28.1 | 420 | 310 | 950 | DC |
| Li et al. (2018) | RC-3 | 12.9 | 0.0 | 200 | 200 | 700* | 170 | 70 | 0.023 | 0.0072 | 38.2 | 359 | 292 | 200 | SC |
| | RC-4 | 22.2 | 0.0 | 200 | 200 | 700 | 170 | 70 | 0.023 | 0.0072 | 38.2 | 359 | 292 | 200 | SC |
| | RC-5 | 9.2 | 0.0 | 200 | 200 | 700 | 170 | 90 | 0.023 | 0.0056 | 38.2 | 359 | 292 | 200 | SC |
| | RC-6 | 13.0 | 0.0 | 200 | 200 | 700 | 170 | 90 | 0.023 | 0.0056 | 38.2 | 359 | 292 | 200 | SC |
| | RC-7 | 15.6 | 0.0 | 200 | 200 | 700 | 170 | 120 | 0.023 | 0.0042 | 38.2 | 359 | 292 | 200 | SC |
| | RC-8 | 16.7 | 0.0 | 200 | 200 | 700 | 170 | 120 | 0.023 | 0.0042 | 38.2 | 359 | 292 | 200 | SC |
| Zhang et al. (2017); Zhang et al. (2015) | C-10-L-0 | 12.7 | 0.0 | 250 | 250 | 600 | 200 | 100 | 0.063 | 0.0063 | 23.8 | 476 | 342 | 180 | SC |
| | C-15-L-0 | 14.6 | 0.0 | 250 | 250 | 600 | 200 | 100 | 0.063 | 0.0063 | 23.8 | 476 | 342 | 180 | SC |
| | C-25-L-0 | 21.7 | 0.0 | 250 | 250 | 600 | 200 | 100 | 0.063 | 0.0063 | 23.8 | 476 | 342 | 180 | SC |
| Lee et al. (2003) | RC-COR-1 | 6.8 | 0.0 | 300 | 300 | 550 | 240 | 80 | 0.027 | 0.0065 | 39.2 | 363 | 347 | 706 | DC |
| | RC-COR-2 | 13.6 | 0.0 | 300 | 300 | 550 | 240 | 80 | 0.027 | 0.0065 | 39.2 | 363 | 347 | 706 | DC |
| | RC-COR-3 | 27.2 | 0.0 | 300 | 300 | 550 | 240 | 80 | 0.027 | 0.0065 | 39.2 | 363 | 347 | 706 | DC |
| Shi et al. (2000) | Z5 | 18.0 | 18.0 | 200 | 200 | 900 | 170 | 80 | 0.023 | 0.0035 | 21.0 | 415 | 235 | 227 | SC |
| | Z7 | 13.7 | 13.7 | 200 | 200 | 900 | 170 | 80 | 0.023 | 0.0035 | 21.0 | 415 | 235 | 227 | SC |

$X_l$ : corrosion level (mass loss) of longitudinal reinforcement; $X_t$ : corrosion level (mass loss) of transverse reinforcement; $b$: column section width; $h$: column section height; $a$: shear span of the column; $s$: center-to-center spacing of transverse reinforcement; $\rho_l$ : longitudinal reinforcement ratio; $\rho_t$ : transverse reinforcement ratio; $f_c^{'}$ : concrete compressive strength; $f_{yl}$ : yield strength of longitudinal reinforcement; $f_{yt}$ : yield strength of transverse reinforcement; $P$: axial load.

* As no value was provided in original literature, this value was assumed.

** SC: single cantilever; DC: double cantilever

### 3.4 Elastic shear stiffness

The elastic shear deformation is usually very small and comprises less than 10% of the total deformation (Sezen and Moehle 2006; LeBorgne and Ghannoum 2014a) for RC column. Therefore in this study, rather than using calibrated elastic shear stiffness from the column database, a simple expression is adopted for the initial elastic shear stiffness $K_e$ :

$$K_e = \frac{5}{6}\frac{G \cdot A_g}{L} = \frac{E_c \cdot A_g}{3L} \tag{17}$$

where $G = E_c / 2(1+\upsilon)$ is the shear modulus; $A_g$ and $L$ are column gross section area and column clear length, respectively; $E_c$ and $\upsilon$ are the elastic modulus and poison ratio of concrete, respectively. Similar consideration of elastic shear stiffness has been used by some other studies (LeBorgne and Ghannoum 2014a).

The limit of the elastic shear response is marked by a yield shear force $V_y$ . Based on the data of the extracted shear response, the yield shear force $V_y$ could be set as 75% of the peak shear capacity $V_n$ . As will be shown later, this simple consideration provides reasonably accurate estimate of the yield shear force and yield shear deformation as compared with test results.

### 3.5 Shear strength

The shear strength $V_n$ defines the maximum shear capacity of the corroded column, and is also the limit value after which the strength deterioration will be triggered in the proposed model.

In the present study, the shear strength for corroded RC columns is determined using the shear strength model proposed by Vu and Li (2018b). This model is based on the shear strength model in ASCE 41-13 (2014) with some modifications to suit corroded conditions. In this shear strength model, the total shear strength $V_n$ comprises two parts: the shear strength provided by transverse reinforcements $V_s$ and the shear strength provided by concrete $V_c$ . As corrosion will reduce the cross-sectional area and yield strength of transverse reinforcement, the shear strength provided by transverse reinforcement is reduced and can be calculated by the modified material parameters as:

$$V_s = \frac{A_{st,cor} f_{yt,cor} d}{s} \tag{18}$$

where, $A_{st,cor}$ is the total cross-sectional area of corroded transverse reinforcement, that can be calculated by Eq. 1; $f_{yt,cor}$ is the yield strength of corroded transverse reinforcement, that can be calculated by Eq. 2; $d$ is the effective depth of column section; $s$ is the center-to-center spacing of transverse reinforcement.

Considering the reduction of the strength of the concrete due to the volumetric expansion caused by steel rust, the shear strength provided by concrete can be estimated as follows:

$$V_c = \left[\frac{0.5\sqrt{f_c'}}{a/d}\sqrt{1+\frac{P}{0.5\sqrt{f_c'}(A_{core}+\sqrt{\zeta}A_{cover})}}\right] \cdot 0.8(A_{core}+\sqrt{\zeta}A_{cover}) \tag{19}$$

where $A_{core}$ is the area of core concrete; $A_{cover}$ is the area of cover concrete; $\zeta$ is the softening coefficient of cover concrete.

Finally, the total shear strength is the summation of shear strength provided by transverse reinforcement and concrete:

$$V_n = V_s + V_c \tag{20}$$

Through the process of shear strength estimation, it can be seen that the corrosion effect on shear strength of corroded columns is reflected in two aspects: the reduced shear strength provided by transverse reinforcement and by cover concrete. The corrosion level is an important parameter in calculating the shear strength of corroded columns. However, according to Vu and Li (2018b), the shear strength calculated using the corrosion level estimated in terms of mass loss (denoted as $X^m$) tends to be overestimated and not conservative. On the other hand, using the corrosion level estimated in terms of minimum residual cross-sectional area (denoted as $X^r$) could provide more reliable results. In this paper, the shear strength will be calculated using $X^r$. As the corrosion level for most of the columns in the collected database has been represented by $X^m$, a conversion relationship is needed to convert $X^m$ to $X^r$. For this purpose, the following empirical correlation from experiment results (Vu and Li 2018b) is adopted:

$$X^r = 1.64X^m + 20.82 \tag{21}$$

Based on Eq. 21, the corrosion level estimated in $X^m$ can be converted to $X^r$, and the shear strength can be calculated with Eq. 20.

The shear strength of the 25 collected corroded columns are calculated using three different methods: method 1 and 2 (designated as M1 and M2) as proposed by Vu and Li (2018b) with different corrosion levels, with M1 using $X^m$ and M2 using $X^r$, and method 3 following the shear strength model in ASCE 41-13 with unmodified material properties. The results are compared with experimental data in Fig. 7. It is evident that the method of ASCE 41-13 significantly overestimates the shear strength for corroded columns. This is expected because this model does not consider the effects of corrosion on shear strength. The mean and coefficient of variation of predicted $V_n$ to test $V_n$ are 1.17, 0.15 for M1 and 0.90, 0.13 for M2, respectively. It can be seen that shear strength calculated using $X^r$ provide more reliable and conservative results.

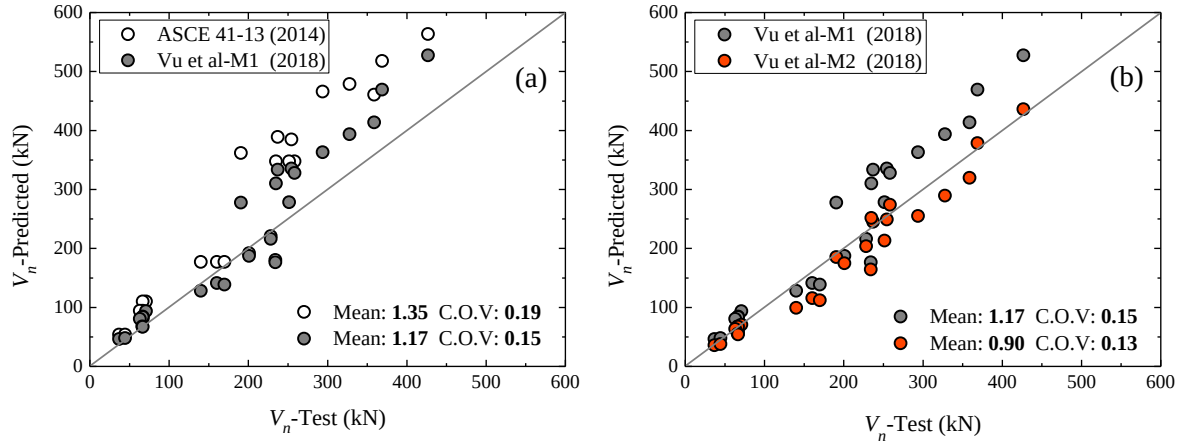


**Fig. 7** Comparison of predicted shear strength with test results: **a** ASCE 41-13 and M1 method; **b** M1 and M2 method

### 3.6 Pre-peak plastic deformation

The pre-peak plastic shear deformation $\Delta_p$ is defined as the deformation between the yield strength and the peak shear strength, as shown in Fig. 3(a). This value can be calibrated directly from the extracted shear response of each column. After obtaining this value, an empirical equation can be developed using regression analysis.

Several candidate predictor variables are considered in this study including column parameters listed in Table 1 and predictor variables used by Lee and Han (2018). A multiplication form is considered for the regression analysis:

$$y = a_0 \cdot (X_1)^{a_1} \cdot (X_2)^{a_2} \cdots (X_n)^{a_n} \tag{22}$$

where $y$ is the target variable; $a_i$ is the constant determined from the regression analyses; $X_i$ is the predictor variable. During the regression analysis, only the statistically significant predictor variables are included in the nonlinear model; a predictor is considered statistically significant if the $p$ value of standard $F$-test is less than 0.05.

For the pre-peak plastic deformation $\Delta_p$, the statistically significant predictor variables are found to be axial load ratio $P/A_g f_c^{'}$, shear span to depth ratio $a/d$ and modified transverse reinforcement strength contribution ratio $(1-X_t)\cdot f_{yt}A_{st}/f_c^{'}A_g$. Normalising the pre-peak plastic deformation $\Delta_p$ with respect to the column shear span $a$, the regression equation is obtained as:

$$\theta_p = \Delta_p / a = 0.12 \cdot \left(\frac{P}{f_c^{'}A_g}\right)^{-0.704} \cdot \left(\frac{a}{d}\right)^{0.653} \cdot \left((1-X_t)\cdot\frac{f_{yt}A_{st}}{f_c^{'}A_g}\right)^{0.984} \tag{23}$$

Fig. 8 shows the comparison between the normalized pre-peak plastic deformation $\theta_p$ as extracted from the experiments and the predicted results using the proposed equation. The determination coefficient $R^2$ is 0.83 which indicates that the proposed equation can predict test values with reasonable accuracy.

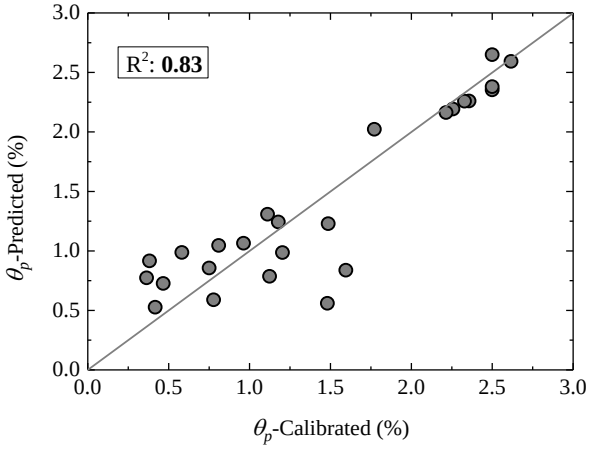


**Fig. 8** Comparison of predicted and calibrated values of $\theta_p$

### 3.7 Post-peak plastic shear deformation

The post-peak plastic deformation $\Delta_{pc}$ is defined as the deformation between the peak shear strength and the point where shear strength reduces to 0, as shown in Fig. 3(a). After the separation of the shear deformation from the test data as explained in Section 3.2, the post-peak plastic shear deformation is extracted from all the 25 colluded columns. This plastic deformation is then normalized with respect to the column shear span $a$. The statistically significant predictor variables are axial load ratio $P/A_g f_c^{'}$, transverse reinforcement spacing to column depth ratio $s/d$ and modified transverse reinforcement ratio $(1-X_t)\rho_t$. With a regression analysis, the following expression is obtained:

$$\theta_{pc} = \Delta_{pc} / a = 0.167 \cdot \left( \frac{P}{f_c^{'} A_g} \right)^{-0.839} \cdot \left( \frac{s}{d} \right)^{-0.033} \cdot \left( (1 - X_t) \rho_t \right)^{0.382} \quad (24)$$

Fig. 9 shows the comparison between the normalized post-peak plastic deformation $\theta_{pc}$ as extracted from the experiments and predicted results using the proposed equation. The determination coefficient $R^2$ is 0.58 which indicates that the proposed equation can predict post-peak plastic deformation of corroded columns with reasonable accuracy.

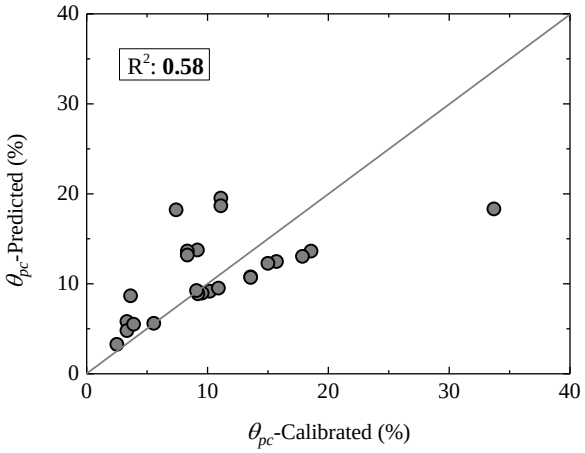


**Fig. 9** Comparison of predicted and calibrated values of $\theta_{pc}$

### 3.8 Cyclic strength and stiffness deteriorations

Under cyclic loading, degradation can occur in peak strength, post-peak strength, reloading stiffness and unloading stiffness. The degradation rate, $\gamma$ , may be set differently for each of the above deterioration properties. However, use of separate $\gamma$ values may not necessarily improve the modeling results remarkably and the overall deterioration effect is not very sensitive to small change of $\gamma$ values (Ibarra et al. 2005; Lignos and Krawinkler 2011). Therefore, $\gamma$ value is set uniformly for the above four deterioration properties for simplicity. The primary calibration criterion is to match the average deterioration for strength observed during the displacement history, and on this basis, subsequent emphasis is placed on matching the deterioration rate of the stiffness.

The regression equation for deterioration parameter $\gamma$ is expressed in Eq. 25. The statistically significant predictor variables are axial load ratio $P / A_g f_c^{'}$ , shear span to depth ratio $a / d$ and modified transverse reinforcement strength contribution ratio $(1 - X_t) \cdot f_{yt} A_{st} / f_c^{'} A_g$ .

$$\gamma = 18 \cdot \left( \frac{P}{f_c^{'} A_g} \right)^{-1.090} \cdot \left( \frac{a}{d} \right)^{1.485} \cdot \left( (1 - X_t) \cdot \frac{f_{yt} A_{st}}{f_c^{'} A_g} \right)^{0.100} \quad (25)$$

Fig. 10 shows the comparison between the $\gamma$ values as extracted from the experiments and the predicted results using the above regression equation. The determination coefficient $R^2$ is 0.79 indicating that the proposed equation can well predict the actual values of parameter $\gamma$ .

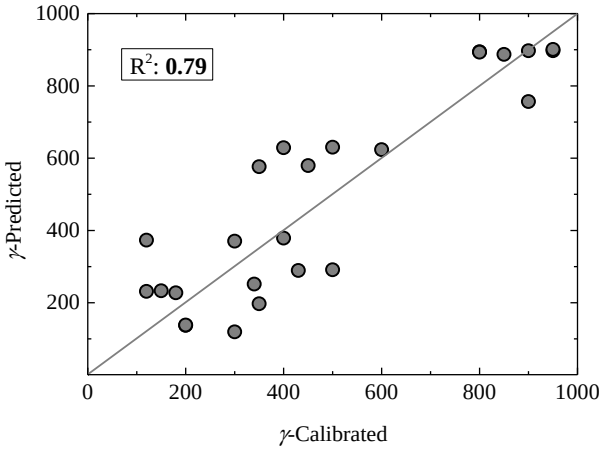


**Fig. 10** Comparison of predicted and calibrated values of deterioration parameter $\gamma$

### 3.9 Pinching parameters

Two pinching related parameters are also calibrated in order to simulate the pinching behavior of corroded columns. The pinching parameter $a_p$ (*APinch* in OpenSEES) defines the ratio of reloading stiffness and $\kappa_{f,d}$ defines the ratio of the load at which reloading begins to the load that corresponds to the maximum historic deformation demand as shown in Fig. 3(b). These two parameters are calibrated in order to match the pinching phenomenon observed for each shear response.

The regression equation for parameter $a_p$ is expressed in Eq. 26. The statistically significant predictor variables are modified transverse reinforcement ratio $(1-X_t)\rho_t$ , modified longitudinal reinforcement strength contribution ratio $(1-X_l)\cdot f_{yl}A_{sl}/f_c^{'}A_g$ . Fig. 11(a) shows the comparison between calibrated $a_p$ and predicted values using the proposed equation. The determination coefficient $R^2$ of the proposed equation is only 0.20, it is mainly because the pinching is highly nonlinear and complex. Thus it is difficult to predict parameter $a_p$ with only limited column parameters.

The parameter $\kappa_{f,d}$ is set to be the same for positive and negative loading directions (Ibarra et al. 2005). The regression equation for $\kappa_{f,d}$ is expressed in Eq. 27. The statistically significant predictor variables are shear span to effective depth ratio $a/d$ , transverse reinforcement spacing to column depth ratio $s/d$ and modified transverse reinforcement strength contribution ratio $(1-X_t)\cdot f_{yt}A_{st}/f_c^{'}A_g$ . Fig. 11(b) shows the comparison between calibrated $\kappa_{f,d}$ and predicted values using the proposed equation. The determination coefficient $R^2$ is 0.74 which indicates that the proposed equation can provide relative good prediction results for $\kappa_{f,d}$ .

$$a_p = 0.25\cdot\left((1-X_t)\rho_t\right)^{0.150}\cdot\left((1-X_l)\cdot\frac{f_{yl}A_{sl}}{f_c^{'}A_g}\right)^{0.170} \tag{26}$$

$$\kappa_{f,d} = 0.663\cdot\left(\frac{a}{d}\right)^{0.778}\cdot\left(\frac{s}{d}\right)^{0.211}\cdot\left((1-X_t)\cdot\frac{f_{yt}A_{st}}{f_c^{'}A_g}\right)^{0.287} \tag{27}$$

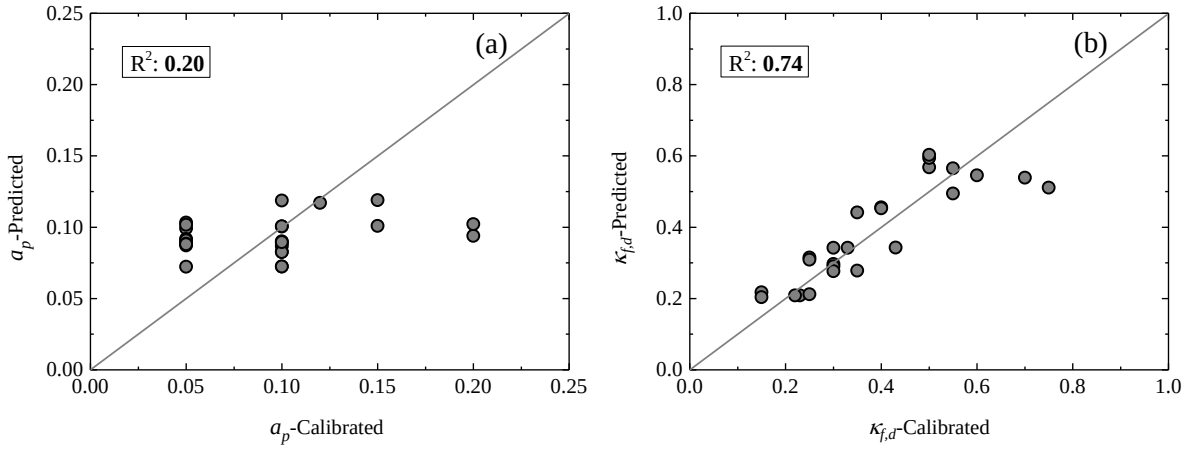


**Fig. 11** Comparison of predicted and calibrated values of pinching parameters: **a** $a_p$ ; **b** $\kappa_{f,d}$

In this study, the residual shear strength $V_r$ is set to be 20% of the peak shear strength (Jeon et al. 2015). Another parameter $\Delta_u$ that defines the ultimate deformation capacity, is highly dependent on the loading histories and varies for columns under different loading proctols (Lignos and Krawinkler 2011). In this study, it is set to be the sum of the post-peak plastic deformation $\Delta_{pc}$, the elastic shear deformation $\Delta_y$ and the pre-peak plastic shear deformation $\Delta_p$.

## 4 Model Verification

With the proposed equations for individual modeling parameters, the shear spring can be defined for RC columns in different corrosion states, and subsequently the overall behavior of the corroded columns can be simulated with the proposed modeling framework. In this section, the analyses of several columns are presented for verifying the accuracy of the proposed model.

### 4.1 Simulation without and with shear deformation and comparison

Firstly, a selected column is simulated with two methods to show the importance of shear response consideration in modeling the seismic behavior of corroded columns. This column is C3 from the tests by Vu and Li (2018a). It was originally ductile-designed but failed in a non-ductile manner due to corrosion.

The column is simulated respectively by: a) considering only flexural behavior (flexure simulated), and b) considering shear behavior in addition to flexural behavior (shear simulated). For the shear simulation, the modeling parameters are obtained from the proposed calibration equations. The main modeling parameters are shown in Fig. 12(a). The experimental displacement loading protocol is followed in both simulations. Fig. 12 presents the comparison of the simulated and test results. The figure exemplifies the difference of flexural simulation and shear simulation for corroded columns failed in shear. As shown in Fig. 12(a), considering only the flexure response overestimates significantly the strength and stiffness, whereas considering the shear behavior gives much improved prediction results. The overall hysteretic behavior is close to the test results. The strength deterioration after the peak load is well captured and the severe pinching behavior can also be well simulated.

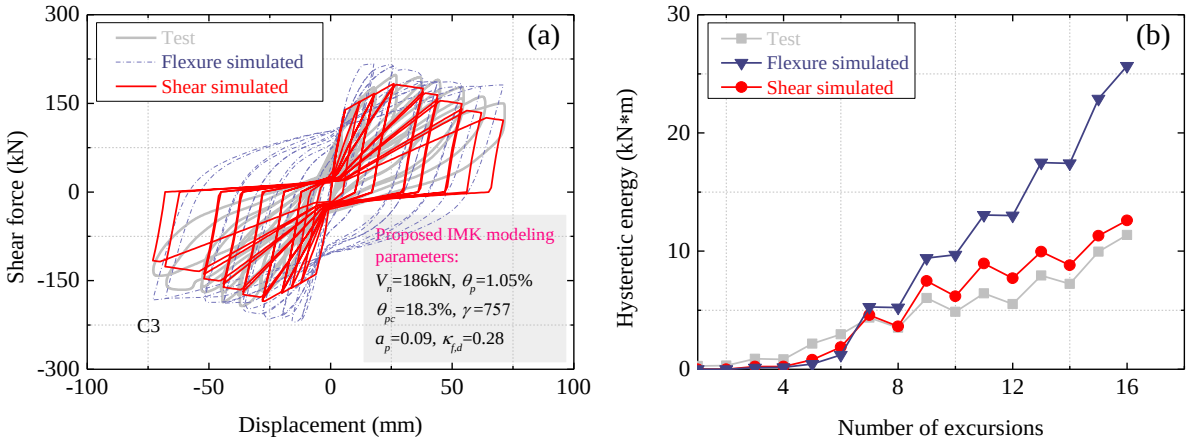


**Fig. 12** Comparison of simulated and test results: **a** hysteretic response; **b** hysteretic energy dissipation

Fig. 12(b) depicts the hysteretic energy dissipation histories for the column. It can be seen that the trend of hysteretic energy dissipation history from shear simulation is close to the test results. The proposed model replicates well the cumulative energy dissipated at almost all the displacement levels. On the contrary, the hysteretic energy from flexural simulation is highly overestimated, especially at large displacement levels. This is mainly because the flexural method cannot well capture the strength deterioration and pinching behaviors of corroded column when the shear capacity is reached.

### 4.2 Ductile-designed columns

In this section, four columns which were originally ductile (flexural)-designed but failed in shear due to corrosion are simulated. Table 2 lists these columns and the main IMK modeling parameters as determined using equations in Section 3.

Fig. 13 shows a comparison between the simulated and experimental lateral force-displacement curves of the corroded columns. It can be observed that overall the proposed model can simulate the hysteretic behaviors of corroded columns reasonably well. The simulated lateral force-displacement curves are close to test results. It should be noted that some experimental curves exhibit asymmetric hysteretic behaviors, this could be because the steel reinforcement of the columns was non-uniformly corroded in the experiment, causing the corroded column to behave differently under positive and negative loadings.

Because of the shear spring, the deterioration behaviors of the columns can be adequately simulated. As illustrated in Fig. 13, even slight strength deterioration and stiffness deterioration before the maximum shear capacity can be well predicted. Upon reaching the maximum shear capacity where shear failure occurs, significant deterioration begins and this is well captured with the proposed model. For the column C5 tested by Vu and Li (2018a), the onset of shear failure is predicted slightly earlier while the post-peak deterioration is slightly over simulated. But overall, the prediction accuracy of the model is acceptable.

The pinching behavior is also well simulated, and this is evident from the severe pinching behavior of column C5 and lesser pinching behavior of column Z5, to the moderate pinching behavior in the rest of the columns. It is worth noting that the prediction accuracy of pinching behavior appears not sensitive to the discrepancy in the estimation of the pinching parameters, thus although the determination coefficient $R^2$ of the equation for pinching parameter $a_p$ is relative low, as

described in Section 3.9, the pinching behavior can still be simulated with reasonable accuracy.

**Table 2** List of selected ductile-designed columns and estimated modeling parameters

| Specimen | $V_n$ (kN) | $\theta_p$ (%) | $\theta_{pc}$ (%) | $\gamma$ | $a_p$ | $\kappa_{f,d}$ |
|---|---|---|---|---|---|---|
| RC4 (Li et al. 2018) | 59.4 | 2.02 | 13.1 | 887 | 0.09 | 0.49 |
| RC6 (Li et al. 2018) | 63.4 | 2.26 | 12.3 | 897 | 0.09 | 0.54 |
| C5 (Vu and Li 2018a) | 245.1 | 0.79 | 8.9 | 289 | 0.10 | 0.31 |
| Z5 (Shi et al. 2000) | 36.7 | 1.24 | 5.5 | 576 | 0.09 | 0.59 |

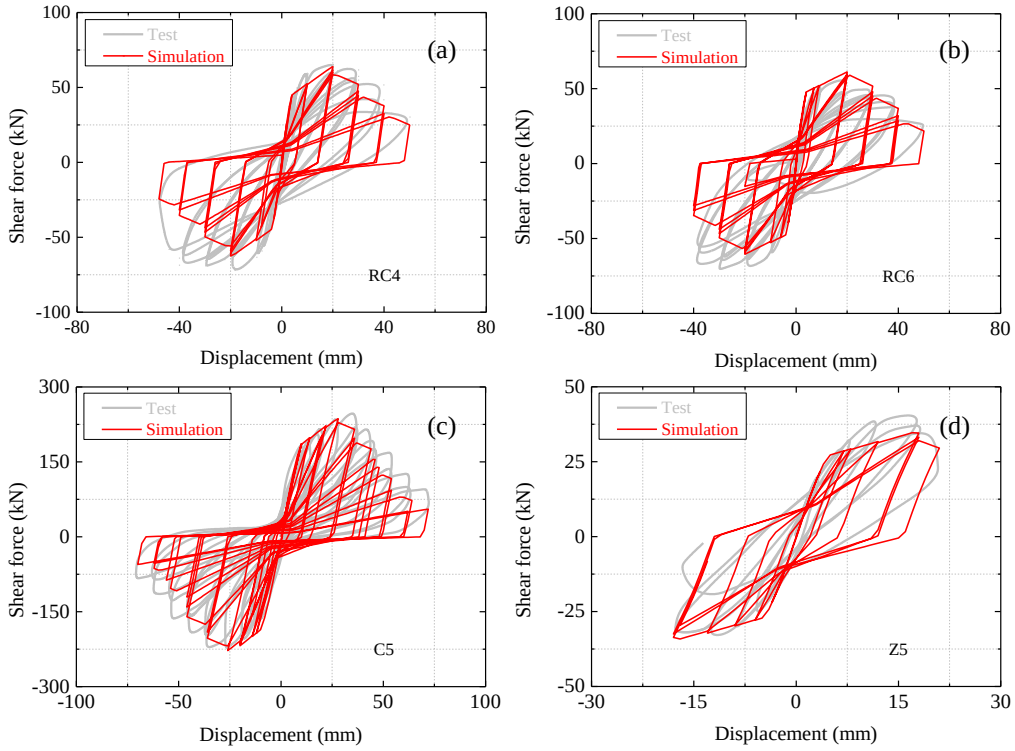


**Fig. 13** Comparison of simulated and experimental cyclic curves for ductile-designed columns

### 4.3 Short shear-critical columns

Four short shear-critical columns from the column database are also selected and simulated to verify the accuracy of the proposed model. These columns are more inclined towards shear-dominated behavior and so provide a further perspective for verifying the accuracy of the shear spring. Table 3 lists the main IMK modeling parameters estimated using the equations in Section 3 for these columns. A comparison of the simulated and experimental lateral force-displacement curves is shown in Fig. 14. The results show that the proposed model can simulate the overall hysteretic behavior of short corroded columns reasonably well. The deterioration process of these short columns can be adequately simulated, with the rate of strength deterioration and stiffness deterioration being close to the test results. All of the four short columns exhibit more serious pinching behavior as compared with ductile-designed columns, and the proposed model can predict such pinching behavior very well.

For columns CC1 and CC2, the peak shear strengths from the simulation are lower than test results, and this could be attributed to the shear strength model being on the conservative side and generally higher uncertainty in the actual shear

strength.

**Table 3** Predicted modeling parameters for short shear-critical columns

| Specimen | $V_n$ (kN) | $\theta_p$ (%) | $\theta_{pc}$ (%) | $\gamma$ | $a_p$ | $\kappa_{f,d}$ |
|---|---|---|---|---|---|---|
| CC1 (Vu and Li 2018b) | 319.7 | 1.23 | 19.5 | 379 | 0.10 | 0.22 |
| CC2 (Vu and Li 2018b) | 289.5 | 0.99 | 18.7 | 370 | 0.10 | 0.20 |
| RC-COR-1 (Lee et al. 2003) | 274.1 | 0.98 | 9.5 | 230 | 0.09 | 0.30 |
| RN3 (Ma et al. 2018) | 203.9 | 0.53 | 3.2 | 120 | 0.07 | 0.34 |

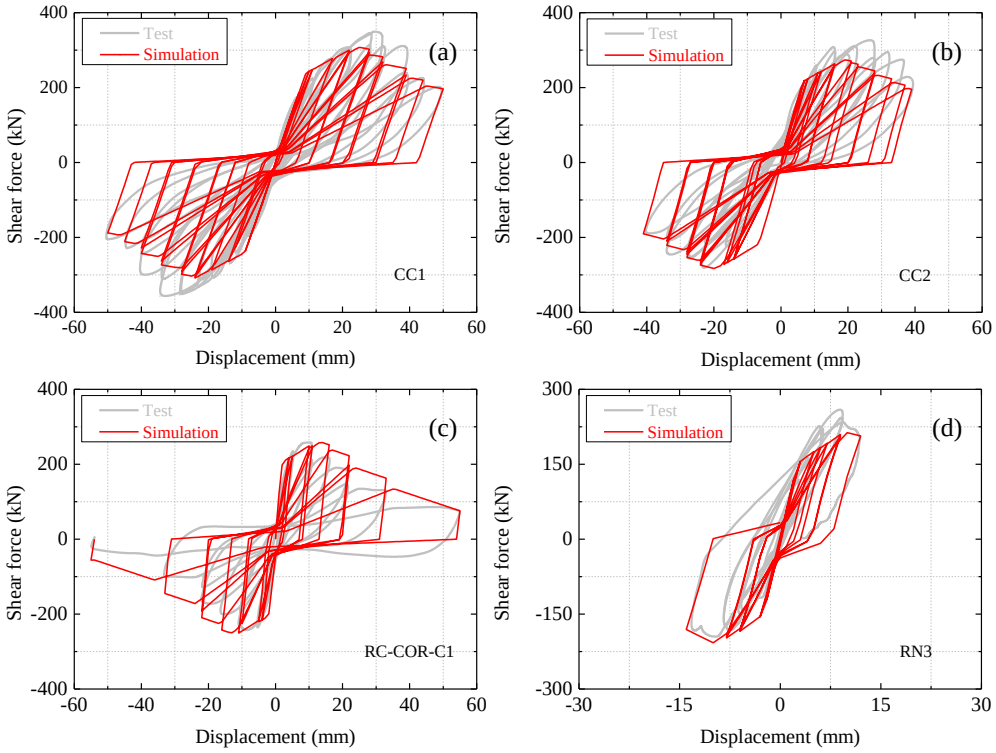


**Fig. 14** Comparison of simulated and test cyclic curves for short shear-critical columns

## 5 Corrosion effects on seismic performance of columns

Based on the proposed model, the effects of corrosion on seismic performance of RC columns can be investigated. In this section, a ductile-designed column is hypothetically subjected to different corrosion levels and modeled with the proposed model to investigate the corrosion effects on seismic performance of RC columns.

The details of the original column are taken from column U1 in the tests conducted by Vu and Li (2018a). This column is 1.78 m in height, and its shear span to depth ratio is 3.18. Four transverse reinforcement corrosion levels are considered, namely 10%, 20%, 30% and 40% (in terms of mass loss as described), and the corresponding column cases are denoted as *X*-10, *X*-20, *X*-30 and *X*-40, respectively. As longitudinal reinforcement is usually less corroded compared with transverse reinforcement, the corrosion levels of longitudinal reinforcements are set to be one third of the respective transverse reinforcement corrosion levels, for an illustrative purpose. The estimated shear capacity $V_n$ and flexural capacity $V_f$ of the columns are shown in Table 4, the variation trend with the corrosion level is shown in Fig. 15(b). The estimated

deterioration modeling parameters are given in Table 4.

The predicted flexural capacity of column U1 and *X*-10 are 276.4 kN and 260.4 kN, while shear capacity are 338.8 kN and 266.1 kN, respectively. Thus, these two columns are anticipated to fail in flexure as the shear capacity is larger than flexural capacity. Due to the higher degree of corrosion of transverse reinforcement, the shear capacity of the column reduces more quickly than the flexural capacity, and consequently, starting from the 20% corrosion level, the predicted shear capacity becomes lower than flexural capacity and this is anticipated to result in a shift of the failure mode towards shear.

Fig. 15(a) presents the monotonic lateral load (shear force) vs. lateral drift curves of the columns. It can be observed that with the increase of the corrosion level, the peak lateral strength decreases significantly. After the peak lateral strength, columns *X*-20, *X*-30 and *X*-40 all exhibit apparent strength deterioration, with a post-peak negative stiffness, and eventually fail in shear. Columns U1 and *X*-10 maintain a ductile post-peak behavior as these two cases are both governed by flexure.

**Table 4** Predicted modeling parameters for columns under various corrosion levels

| Specimen | $X_t$ (%) | $X_l$ (%) | $V_n$ (kN) | $V_f$ (kN) | $\theta_p$ (%) | $\theta_{pc}$ (%) | $\gamma$ | $a_p$ | $\kappa_{f,d}$ |
|---|---|---|---|---|---|---|---|---|---|
| U1 | 0 | 0 | 338.8 | 276.4 | 1.72 | 20.4 | 796 | 0.10 | 0.32 |
| *X*-10 | 10 | 3.5 | 266.1 | 260.4 | 1.56 | 19.6 | 787 | 0.10 | 0.31 |
| *X*-20 | 20 | 7.0 | 218.0 | 251.3 | 1.38 | 18.7 | 778 | 0.10 | 0.30 |
| *X*-30 | 30 | 10 | 177.6 | 241.1 | 1.21 | 17.8 | 768 | 0.10 | 0.28 |
| *X*-40 | 40 | 13.5 | 144.7 | 230.4 | 1.04 | 16.7 | 756 | 0.10 | 0.27 |

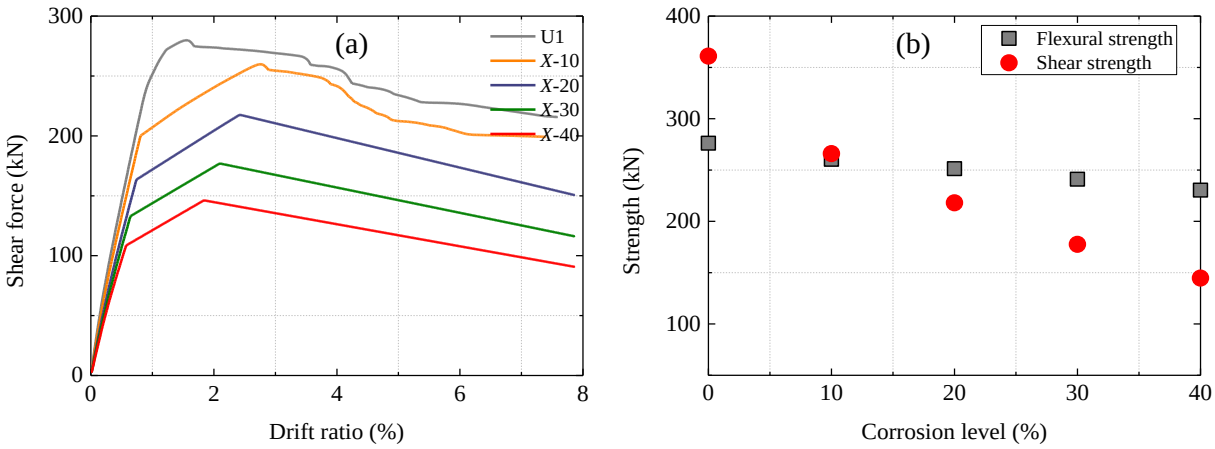


**Fig. 15** Comparison of predicted backbone curves and lateral strength of columns with various corrosion levels

The dynamic performance of the columns are also investigated. For the dynamic analysis, the axial dead load including self-weight is represented by a lumped mass at the column top, and the amount of mass is 39,715kg. The ground motion of the 2009 L'Aquila, Italy Earthquake recorded at *L'Aquila-V.Aterno-Centro Valle* station is used as the excitation, with a PGA equal to 0.56g. A 2% Rayleigh damping is used during the analysis.

Fig. 16 and Fig. 17 show the time histories of the drift and base shear responses of columns U1 and *X*-30, representing a flexure- and a shear-dominated failure mode, respectively. It can be observed that the corroded column *X*-30 exhibits a smaller base shear and a much larger drift response as compared with the original column U1. The maximum drift ratio of column *X*-30 is 6.9% while it is only 3.2% for column U1.

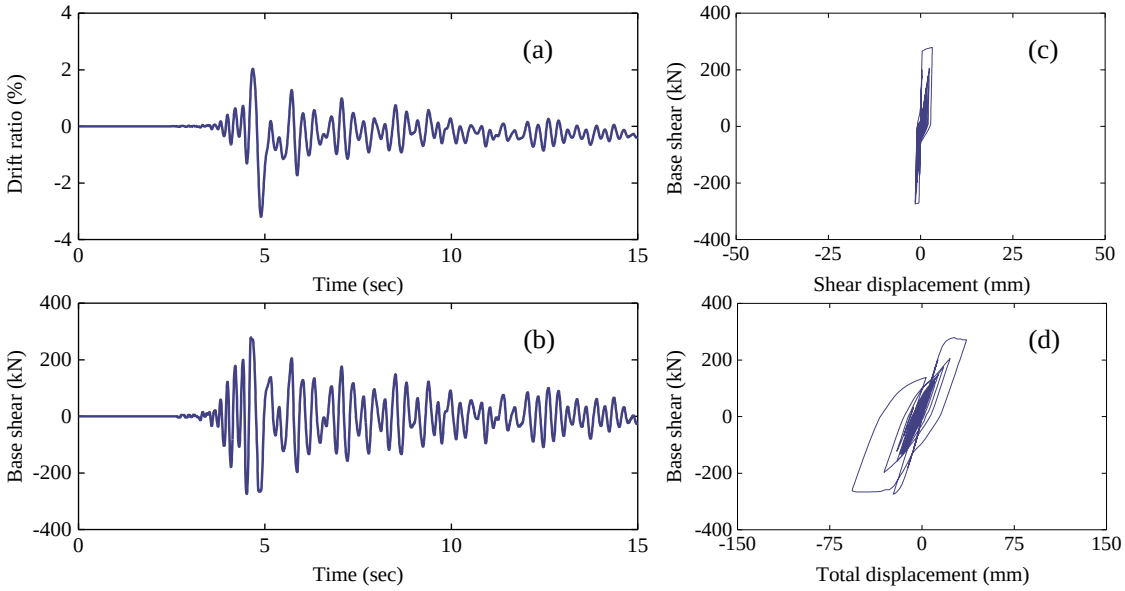


**Fig. 16** Seismic response of pristine column U1: **a** drift response; **b** base shear; **c** shear hysteretic response; **d** total hysteretic response

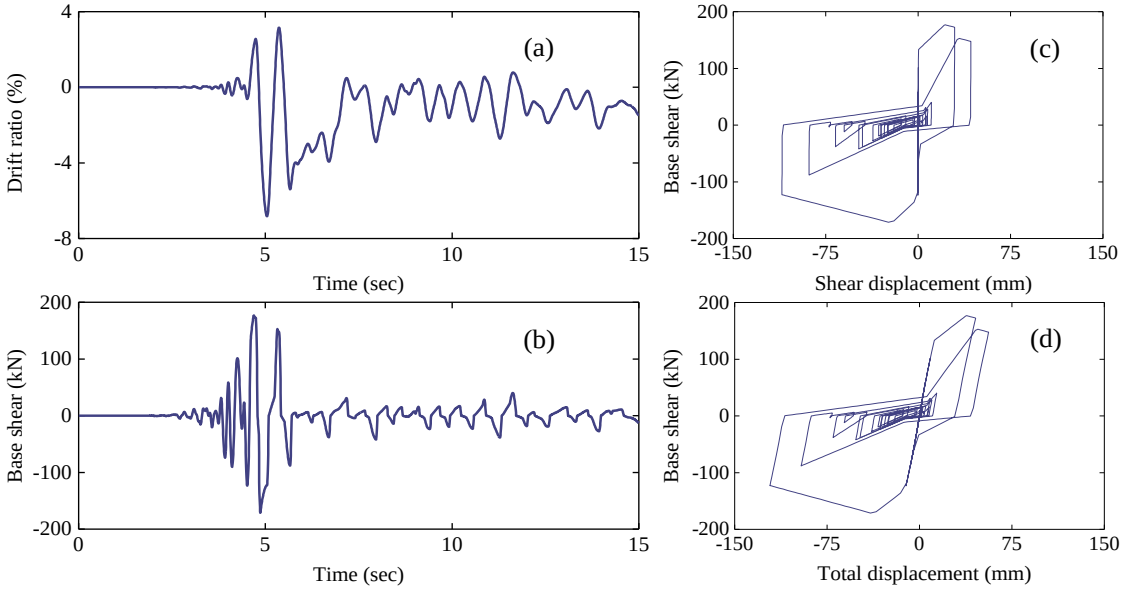


**Fig. 17** Seismic response of column *X*-30: **a** drift response; **b** base shear; **c** shear hysteretic response; **d** total hysteretic response

Fig. 16 and Fig. 17 also present the hysteretic response of the two columns. The shear hysteretic response of the columns are also plotted. It can be seen that the un-corroded column U1 has much smaller shear displacement comparing with the corroded case *X*-30. The maximum shear displacement of column U1 is approximately 3.2mm, 8.7% of the total displacement. In contrast, for column *X*-30, the maximum shear displacement is approximately 110mm, 90% of the total displacement. It is evident that for column failed in shear, the shear displacement dominates the total displacement response. Because of the corrosion of transverse reinforcement, shear capacity deteriorates and shear response becomes more significant. Thus, it is very important to consider the shear response and the potential of a shear failure for seismic performance assessment of corroded columns.

## 6 Conclusions

This paper presents an analytical model for seismic performance assessment of corroded reinforced concrete columns. The model takes into account the shear capacity deterioration due to the corrosion suffered by the transverse reinforcement, and the flexure-shear interaction behavior in a coupled manner. This is achieved through the incorporation of a new macro zero-length shear spring element in series with a flexural column element and a rotational slip element. The effect of corrosion on flexural behavior is considered by means of the modification of steel reinforcement, concrete material and bond properties. For the shear behavior, the modified Ibarra-Medina-Krawinkler deterioration model is employed to capture different aspects of deterioration, including the basic strength deterioration, in-cycle strength deterioration, stiffness deterioration and pinching. Empirical equations for the determination of the modeling parameters of the shear spring are proposed based on calibration against a collected corroded column database where all columns failed in shear. The equations are established through regression analyses in relation to the statistically significant predictor variables. The model is verified through numerical simulation of several columns from the dataset, and the corrosion effects on the seismic performance of RC columns are investigated with the proposed model. Based on the results, some conclusions can be drawn as below:

Comparison of the predicted and test results for several corroded RC columns shows that the proposed model is able to predict the overall hysteretic behaviors with reasonably accuracy. Detailed deterioration process and pinching effect can be well replicated for ductile-designed corroded columns as well as short shear-critical corroded columns. Compared with flexural simulation, simulation considering shear response can more closely reproduce test results for corroded columns failed in shear.

Corrosion can lead to significant shear capacity deterioration, and as a result, an originally ductile-designed column can shift to a shear-dominate behavior with significant deterioration behavior. Therefore, it is important to take the shear behavior into consideration in the seismic performance assessment of corroded RC columns.

Further study is required to broaden the column database and extend the coverage range of the empirical estimation equations for the determination of the modeling parameters for the shear spring element.

## Acknowledgments

The authors acknowledge financial support from the National Key Research and Development Program of China (No. 2016YFC0701100, No. 2016YFC0701400) and the National Natural Science Foundation of China (No. 51525801). The financial support from China Scholarship Council (No. 201706090085) is also gratefully acknowledged. The opinions and conclusions presented in this paper are those of the authors and do not necessarily reflect the views of the sponsoring organizations.

## References

Afsar Dizaj E, Madandoust R, Kashani MM (2017) Exploring the impact of chloride-induced corrosion on seismic damage limit states and residual capacity of reinforced concrete structures. Struct Infrastruct Eng 14(6):1-16

ASCE (2014) Seismic evaluation and retrofit of existing buildings. ASCE 41-13, Reston, VA. .

Cassese P, De Risi MT, Verderame GM (2018) A modelling approach for existing shear-critical RC bridge piers with hollow rectangular cross section under lateral loads. Bull Earthq Eng 17(1):237-270

D'Ambrisi A, Filippou FC (1999) Modeling of cyclic shear behavior in RC members. J Struct Eng 125(10):1143-1150

Di Carlo F, Meda A, Rinaldi Z (2017a) Numerical evaluation of the corrosion influence on the cyclic behaviour of RC columns. Eng Struct 153:264-278

Di Carlo F, Meda A, Rinaldi Z (2017b) Numerical cyclic behaviour of un-corroded and corroded RC columns reinforced with HPFRC jacket. Compos Struct 163:432-443

Du Y, Clark L, Chan A (2005a) Effect of corrosion on ductility of reinforcing bars. Mag Concr Res 57(7):407-419

Du Y, Clark L, Chan A (2005b) Residual capacity of corroded reinforcing bars. Mag Concr Res 57(3):135-147

Elwood KJ (2004) Modelling failures in existing reinforced concrete columns. Can J Civ Eng 31(5):846-859

Elwood KJ, Eberhard MO (2009) Effective stiffness of reinforced concrete columns. ACI Struct J 106(4):476-484

Feng DC, Wu G, Sun ZY, Xu JG (2017) A flexure-shear Timoshenko fiber beam element based on softened damage-plasticity model. Eng Struct 140:483-497

Feng DC, Xu J (2018) An efficient fiber beam-column element considering flexure-shear interaction and anchorage bond-slip effect for cyclic analysis of RC structures. Bull Earthq Eng 16(11):1-28

Feng DC, Xie SC, Deng WN, Ding ZD (2019a) Probabilistic failure analysis of reinforced concrete beam-column sub-assemblage under column removal scenario. Eng Fail Anal 100:381-392

Feng DC, Wang Z, Wu G (2019b) Progressive collapse performance analysis of precast reinforced concrete structures. Struct Design Tall Spec Build 28(5):e1588

Gokkaya BU, Baker JW, Deierlein GG (2017) Estimation and impacts of model parameter correlation for seismic performance assessment of reinforced concrete structures. Struct Saf 69:68-78

Goksu C, Ilki A (2016) Seismic behavior of reinforced concrete columns with corroded deformed reinforcing bars. ACI Struct J 113(5):1053-1064

Haselton CB, Liel AB, Deierlein GG, Dean BS, Chou JH (2011) Seismic collapse safety of reinforced concrete buildings. I: assessment of ductile moment frames. J Struct Eng 137(4):481-491

Hsu TT, Mo YL (2010) Unified theory of concrete structures, John Wiley & Sons.

Ibarra LF, Medina RA, Krawinkler H (2005) Hysteretic models that incorporate strength and stiffness deterioration. Earthq Eng Struct Dyn 34(12):1489-1511

Jeon JS, Lowes LN, DesRoches R, Brilakis I (2015) Fragility curves for non-ductile reinforced concrete frames that exhibit different component response mechanisms. Eng Struct 85:127-143

Kashani MM (2014) Seismic performance of corroded RC bridge piers: development of a multi-mechanical nonlinear fibre beam-column model. Ph.D. thesis, Univ. of Bristol, Bristol, U.K

LeBorgne MR, Ghannoum WM (2014a) Calibrated analytical element for lateral-strength degradation of reinforced concrete columns. Eng Struct 81:35-48

LeBorgne MR, Ghannoum WM (2014b) Analytical element for simulating lateral-strength degradation in reinforced concrete columns and other frame members. J Struct Eng 140(7):04014038

Lee CS, Han SW (2018) Computationally effective and accurate simulation of cyclic behaviour of old reinforced concrete columns. Eng Struct 173:892-907

Lee DH, Elnashai AS (2001) Seismic analysis of RC bridge columns with flexure-shear interaction. J Struct Eng 127(5):546-553

Lee H-S, Noguchi T, Tomosawa F (2002) Evaluation of the bond properties between concrete and reinforcement as a function of the degree of reinforcement corrosion. Cem Concr Res 32(8):1313-1318

Lee HS, Kage T, Noguchi T, Tomosawa F (2003) An experimental study on the retrofitting effects of reinforced concrete columns damaged by rebar corrosion strengthened with carbon fiber sheets. Cem Concr Res 33(4):563-570

Lee H, Noguchi T, Tomosawa F (1998) FEM analysis for structural performance of deteriorated RC structures due to rebar corrosion. Proceedings of the Second International Conference on Concrete under Severe Conditions:327-336

Li Q, Niu DT, Xiao QH, Guan X,Chen SJ (2018) Experimental study on seismic behaviors of concrete columns confined by corroded stirrups and lateral strength prediction. Constr Build Mater 162:704-713

Liel A, Haselton C, Deierlein G (2011) Seismic collapse safety of reinforced concrete buildings. II: comparative Assessment of nonductile and ductile moment frames. J Struct Eng 137(4):492-502

Lignos D, Krawinkler H (2008) Sidesway collapse of deteriorating structural systems under earthquake excitations. Rep. No. TB 172, The John A. Blume Earthquake Engineering Center, Stanford Univ., Stanford, CA

Lignos DG, Krawinkler H (2011) Deterioration modeling of steel components in support of collapse prediction of steel moment frames under earthquake loading. J Struct Eng 137(11):1291-1302

Ma G, LiH, Hwang HJ (2018) Seismic behavior of low-corroded reinforced concrete short columns in an over 20-year building structure. Soil Dyn Earthq Eng 106:90-100

Ma Y, Che Y, Gong J (2012) Behavior of corrosion damaged circular reinforced concrete columns under cyclic loading. Constr Build Mater 29:548-556

Mazzoni S, McKenna F, Scott MH, Fenves GL (2006) OpenSees command language manual. Pacific Earthquake Engineering Research (PEER) Center

Meda A, Mostosi S, Rinaldi Z, Riva P (2014) Experimental evaluation of the corrosion influence on the cyclic behaviour of RC columns. Eng Struct 76:112-123

Park R, Priestley M, Gill WD (1982) Ductility of square-confined concrete columns. J Struct Div 108(4):929-950

Rahnama M, Krawinkler H (1993), Effects of soft soil and hysteresis model on seismic demands, John A. Blume Earthquake Engineering Center Standford.

Setzler EJ, Sezen H (2008) Model for the lateral behavior of reinforced concrete columns including shear deformations. Earthq Spectra 24(2):493-511

Sezen H, Moehle JP (2006) Seismic tests of concrete columns with light transverse reinforcement. ACI Struct J 103(6):842-849

Shi QX, Niu DT, Yang GY(2000) Experimental research on hysteretic characteristics of corroded RC members with flexural and compressive axial loads under repeated horizontal loading. Earthq Eng Eng Vib 20(4):44-50 (in Chinese)

Vu NS, Y B, Li B (2016) Prediction of strength and drift capacity of corroded reinforced concrete columns. Constr Build Mater 115:304-318

Vu NS, Li B (2018a) Seismic performance of flexural reinforced concrete columns with corroded reinforcement. ACI Struct J 115(5):1253-1266

Vu NS, Li B (2018b) Seismic performance assessment of corroded reinforced concrete short columns. J Struct Eng 144(4):04018018

Yang SY, Song XB, Jia HX, Chen X, Liu XL (2016) Experimental research on hysteretic behaviors of corroded reinforced concrete columns with different maximum amounts of corrosion of rebar. Constr Build Mater 121:319-327

Zhang C, Zhang DW, Zhao YX, Duan A, Cheng J (2015) Experimental study on seismic behavior of corroded reinforced concrete column wrapped with PET sheet. J Build Struct 36(S2):209-215 (in Chinese)

Zhang DW, Zhao Y, Jin W, Ueda T, Nakai H (2017) Shear strengthening of corroded reinforced concrete columns using pet fiber based composties. Eng Struct 153:757-765